Received: 5 November 2018 | Revised: 13 February 2019 | Accepted: 22 March 2019

DOI: 10.1002/jlcr.3731

RESEARCH ARTICLE

WILEY Journal of Labelled Compounds and Radiopharmaceuticals

Synthesis, ^{3}H-labelling and in vitro evaluation of a substituted dipiperidine alcohol as a potential ligand for chemokine receptor 2

Markus Artelsmair[1] | Patricia Miranda-Azpiazu[2] | Lee Kingston[1] | Jonas Bergare[1] | Magnus Schou[3] | Andrea Varrone[2] | Charles S. Elmore[1]

[1] Early Chemical Development, Pharmaceutical Sciences, IMED Biotech Unit, AstraZeneca, Gothenburg, Sweden

[2] Department of Clinical Neuroscience, Centre of Psychiatry Research, Karolinska Institutet and Stockholm County Council, Stockholm, Sweden

[3] PET Science Centre, Precision Medicine and Genomics, IMED Biotech Unit, AstraZeneca, Karolinska Institutet, Stockholm, Sweden

Correspondence
Markus Artelsmair, Early Chemical Development, Pharmaceutical Sciences, IMED Biotech Unit, AstraZeneca, Pepparedsleden 1, 431 50 Mölndal, Sweden.
Email: markus.artelsmair@astrazeneca.com

Funding information
H2020 Marie Sklodowska-Curie Actions, Grant/Award Number: 675417

The immune system is implicated in the pathology of neurodegenerative disorders. The C-C chemokine receptor 2 (CCR2) is one of the key targets involved in the activation of the immune system. A suitable ligand for CCR2 could be a useful tool to study immune activation in central nervous system (CNS) disorders. Herein, we describe the synthesis, tritium radiolabelling, and preliminary *in vitro* evaluation in *post-mortem* human brain tissue of a known potent small molecule antagonist for CCR2. The preparation of a tritium-labelled analogue for the autoradiography (ARG) study gave rise to an intriguing and unexpected side reaction profile through a novel amination of ethanol and methanol in the presence of tritium. After successful preparation of the tritiated radioligand, *in vitro* ARG measurements on human brain sections revealed nonspecific binding properties of the selected antagonist in the CNS.

KEYWORDS
autoradiography, CCR2, CCR2 antagonist, CNS, radiolabelling, synthesis, tritium

1 | INTRODUCTION

White blood cells or leukocytes are an integral part of the immune system and protect the host organism by patrolling for infectious pathogens and tissue damage. This action is guided by a family of small signalling proteins called chemokines (chemotactic cytokines)[1,2] and their corresponding receptors. Chemokines regulate innate as well as adaptive immune responses by coordinating development, differentiation, anatomic distribution, effector functions, and trafficking of leukocytes.[3] In addition, chemokines cover tasks ranging from lymphocyte development and homing[4,5] to neuronal communication.[6,7] Their physiological effect is derived from interaction with specific G protein–coupled receptors (GPCRs)—transmembrane receptors that are sometimes also referred to as serpentine receptors because the single polypeptide chain winds through the membrane seven times—called chemokine receptors. To date, approximately 50 human chemokines and 20 receptors have been identified, which have traditionally been divided into four families (CXC, CC, C, and CX3C) on the basis of the

pattern of amino acid residues near the $-NH_2$ terminus of the ligands (C stands for cysteine, and X/X3 represents one or three noncysteine amino acids respectively).[8] C-C chemokine receptor 2 (CCR2) is expressed on dendritic cells, endothelial cells and T cells. It is the primary chemokine receptor on inflammatory monocytes and it mediates migration towards chemokines such as CCL2, its primary ligand. However, CCR2 has been implicated in a variety of diseases including atherosclerosis,[9-11] asthma[12,13] and autoimmune[14-16] and metabolic diseases[17] as well as neurological diseases such as neuropathic pain[18] and Alzheimer's disease (AD).[19] Various pharmaceutical companies have tried to identify CCR2 antagonists to therapeutically target one or several of these implications.[20-22] Hurdles in their development have been plentiful, including discrepancies in the activity obtained in the rodent compared with the human receptor, ineffective dosing, and selectivity issues, as antagonists often exhibit high affinities for other chemokine receptors, especially CCR5 and CCR1, as well as ion channels, including hERG.[22-24] Nonetheless, the CCR2/CCL2 axis remains an attractive target with several clinical trials currently ongoing.*

Parkinson's disease (PD) is one of the most common neurodegenerative disorders and is becoming of increasing relevance to the ageing populations of the developed world.[25,26] While a vast number of investigations and discussions around the involvement of CCR2 in inflammatory conditions such as atherosclerosis have been published over the past two decades, its potential importance in PD has primarily been highlighted in more recent years.[27-30] The evident upregulation of CCR2 in PD and the lack of clarity regarding its precise involvement in the pathogenesis of the disease combined with the increasing importance of PD in modern society warrant further studies into CCR2 as a potential targetable biomarker for imaging purposes.[31,32]

Moreover, among a range of cytokines, chemokines, and growth factors examined in a recent study of multiple-system atrophy cerebellar-type (MSA-C) patients by Yamasaki et al, only CCL2 had a significant negative correlation with disease duration.[33]

With regard to AD, an aggressive transgenic model of AD demonstrated that a deficiency in CCR2 accelerated disease progression and increased mortality.[19] However, a recently published 2-year study by Lee et al indicated that increased-plasma CCL2 levels could be associated with increased severity as well as more rapid cognitive decline.[34] These and several other scientific reports highlight the complex role of CCR2 in AD, warranting investigations into this potentially important therapeutic target in the central nervous system (CNS).[35]

Therefore, we set out to study a potential radioligand for imaging CCR2 *in vitro* with the possibility of translating said ligand for *in vivo* molecular imaging with positron emission tomography (PET). *In vivo* PET imaging allows addressing questions central to drug development, for instance, through bio-distribution studies to assess whether the target tissue is reached in sufficient drug quantities for pharmacological efficacy, which is crucial for CNS disorders. Furthermore, provided with the adequate parameters, target occupancy relative to drug plasma concentration can be established, which in turn can be used to direct dose selection. As a result, PET imaging can reduce the attrition of new drugs, particularly in late development stages. The cost of bringing a new drug from its synthesis to the clinical market is approximately 1 billion USD,[36-39] and the time required for clinical development of CNS drug compounds is particularly long—at approximately 8.1 years (10 years if the approval phase is included).[39] Therefore, a radioligand for an important target such as CCR2 could be of significant value to neuroscience research and aid the development of new medicines for the CNS.

2 | RESULTS AND DISCUSSION

2.1 | Antagonist selection

Efforts by various pharmaceutical companies have yielded a wide range of small molecule antagonists with several showing nanomolar or even sub-nanomolar binding affinities for CCR2. A few promising drug candidates are shown in Figure 1. Compound **1**, also known as AZ12567889, has been reported by AstraZeneca to stand out because of its highly potent rodent affinity as well as good pharmacokinetic properties including CNS penetration.[40] Furthermore, it has been used in a preclinical model of neuropathic pain to reverse hyperalgesia.[41] Compounds **2** (INCB8761/PF-4136309)[42] and **3** (INCB3284)[43] both exhibited potent hCCR2 activity, combined with high selectivity over other chemokine receptors and GPCRs and reasonable oral bioavailability. Johnsson & Johnsson disclosed the development of a number of substituted dipiperidine alcohols as potent CCR2 antagonists.[44] The key compound, with an hCCR2 IC_{50} of just 2.4 ($\pm$2.0) nM, showed high selectivity against CCR1, CCR3, CCR4, CCR5, CCR6, CCR7, and CCR8.[45]

While it was primarily considered for the therapy of inflammatory conditions outside the CNS—showing significant *in vivo* efficacy in adjuvant-induced arthritis,

*https://clinicaltrials.gov/ct2/show/NCT02345408, https://adisinsight.springer.com/drugs/800026843

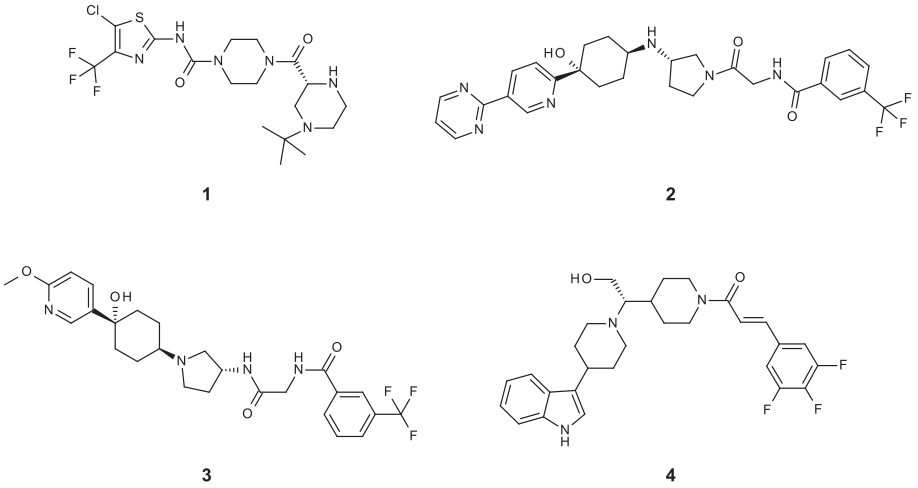

FIGURE 1 Selected drug candidates with IC_{50} values for the C-C chemokine receptor 2 below 10 nM

collagen-induced arthritis and allergic asthma models—it also appeared as a promising candidate for use in the human brain. Compound **4** adhered rather well to the Lipinski's rule of 5,[46] and based on the sum of oxygen and nitrogen atoms, it appeared to have a better chance of passing the blood-brain barrier (BBB) than other candidates. Furthermore, it offered a superior binding affinity for CCR2 as well as the option to introduce both $^{[18]}$F and $^{[11]}$C into the molecule without having to alter the structure. The molecular structures of the other three candidates solely allow for the use of $^{[11]}$C, since they do not feature aromatic fluorine but rather trifluoromethyl groups. While these are amenable to labelling with $^{[18]}$F, the specific activity that can be achieved remains lower than desirable for studying receptors or other low-density targets, despite recent improvements.[47]

To further investigate the potential of compound **4**, it was synthesised according to the procedure of Xia et al[45] (see Section 4).

Its antagonist and agonist potential against hCCR2 and hCCR5 were measured, confirming both the IC_{50} values for hCCR2 and the selectivity over CCR5 with which it shares 75% homology.[48] Based on these results, **4** was chosen as a tritiation target in order to perform autoradiography (ARG) on human brain sections.

2.2 | Iodination and deuteration

The indole moiety was deemed most suitable for labelling *via* a facile tritio-dehalogenation protocol. As the preparation of the CCR2 antagonist **4** was performed on a small scale, only very limited amounts of it were immediately available. However, the multi-step synthesis of **4** proceeds *via* intermediate **5** (shown in Scheme 1), which was present in abundance and ready to use. Furthermore, it has been reported in the literature that under standard reaction conditions for tritio-dehalogenations, using Pd/C and tritium gas, C═C double bonds may undergo saturation or isomerisation,[49,50] even at low tritium pressures.[51] Intermediate **5**, unlike **4**, does not contain a double bond and, therefore, did not appear at risk to undergo an unwanted reduction. Based on the original synthesis by Xia et al,[45] a straightforward route to [^{3}H]**4** was envisioned, in which the alkene moiety would be introduced after incorporating tritium. This option seemed to minimise the inherent risk and could be directly implemented without the need to synthesise more of **4**.

As expected, the iodination of **5** using *N*-iodosuccinimide (NIS) yielded a mixture of regio-isomers with the iodination occurring at several positions on the indole ring. While challenging, it was possible to separate the major isomer **6** (see Scheme 1) using mass-directed

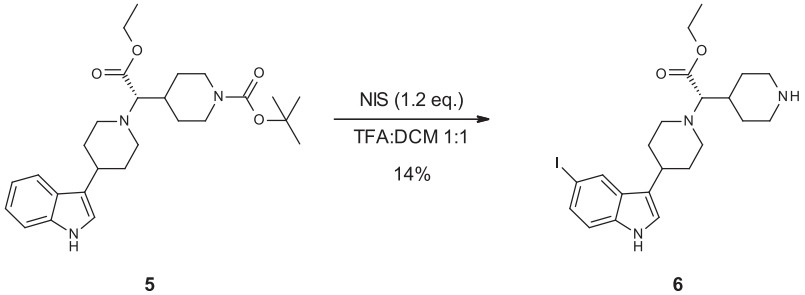

SCHEME 1 Synthesis of the iodinated precursor **6** for subsequent tritium labelling. The yield of just 14% is explained by the challenging separation of the regio-isomers formed, only one of which was used further

supercritical fluid chromatography (SFC-MS). The structural configuration of the major isomer was determined by NMR, in particular nuclear Overhauser effect spectroscopy (NOESY) and rotating frame nuclear Overhauser effect spectroscopy (ROESY). It may be worth noting that reducing the ethyl ester before the iodination was not pursued as, in that case, the separation of the regio-isomers after the iodination was unsuccessful (see Section 4, compound **14**).

To swiftly confirm the feasibility of the reaction sequence from **6** to [^{3}H]**4** (outlined in Scheme 2), it was first tried with deuterium. The first step using deuterium gas and 10% Pd/C proceeded with a good conversion rate of about 80%. The lithium aluminium hydride reduction appeared challenging because of the small reaction scale; nevertheless, the desired product (**4**-d_1) could be formed successfully, as evidenced by LCMS. This encouraged us to pursue this path further and repeat the sequence using tritium.

2.3 | Tritium radiolabelling

Interestingly, it was found that after the first step, namely, the tritio-dehalogenation of **6**, the major product was not the desired compound. That would have had an MS ES$^+$ peak at 372 *m/z*; yet, instead, a peak with a distinct pattern showing 398, 400, 402, 404, 406, and 408 *m/z* was observed. Another noticeably smaller peak exhibited a similar MS pattern with 384, 386, 388, and 390 *m/z*. The approximate ratio by high-performance liquid chromatography (HPLC) was 15:1 (by UV at 280 nm), assuming that, at 280 nm, the indole remains the primary source of absorption. Clearly, an unexpected side reaction was taking place, calling for further investigation into the process. The two main reaction products were isolated by preparative HPLC; and ^{1}H NMR and ^{3}H NMR spectra were taken for both samples.

On the basis of the combined evidence from LCMS and NMR measurements, we propose that a very small fraction of the solvent was oxidised from ethanol to ethanal. This aldehyde then reacted with the secondary amine of the piperidine moiety of **6** to form the iminium ion as outlined in Figure 2. Subsequently, this iminium ion functionality was reduced in the presence of tritium gas yielding the *N*-ethylated derivative (cf Figure 3) of the expected product (**7**).

At this point, it might be worth noting that the initial deuterium trial reaction, which was performed thrice to present a meaningful comparison, consistently showed 80% to 85% (by UV) conversion to the desired product. However, LCMS analysis indicated that 15% to 20% was converted to what appeared to be the *N*-ethylated side product (no methanol was used in this instance). We are not certain of the reason for this considerable difference in reactivity. Perhaps, it was due to an unexplained isotopic effect or the fact that the reaction conditions could not be perfectly reproduced in the tritium experiment.

It was first observed that alcohols are oxidised by Pd(II), or at least that Pd(II) is reduced to Pd(0) in the presence of alcohol, when Berzelius noted that metal precipitate was formed out of a heated alcoholic solution of Pd(II) in 1828.[52] Pd/C generally contains a mixture of Pd(0) and Pd(II) species, and Pd/C with varying reduction degrees is commercially available.[53] Furthermore, palladium on charcoal has extensively been used for the aerobic oxidation of alcohols.[54] Since the catalyst was in ethanol and exposed to air prior to the freeze-thawing cycles, this could have taken place.

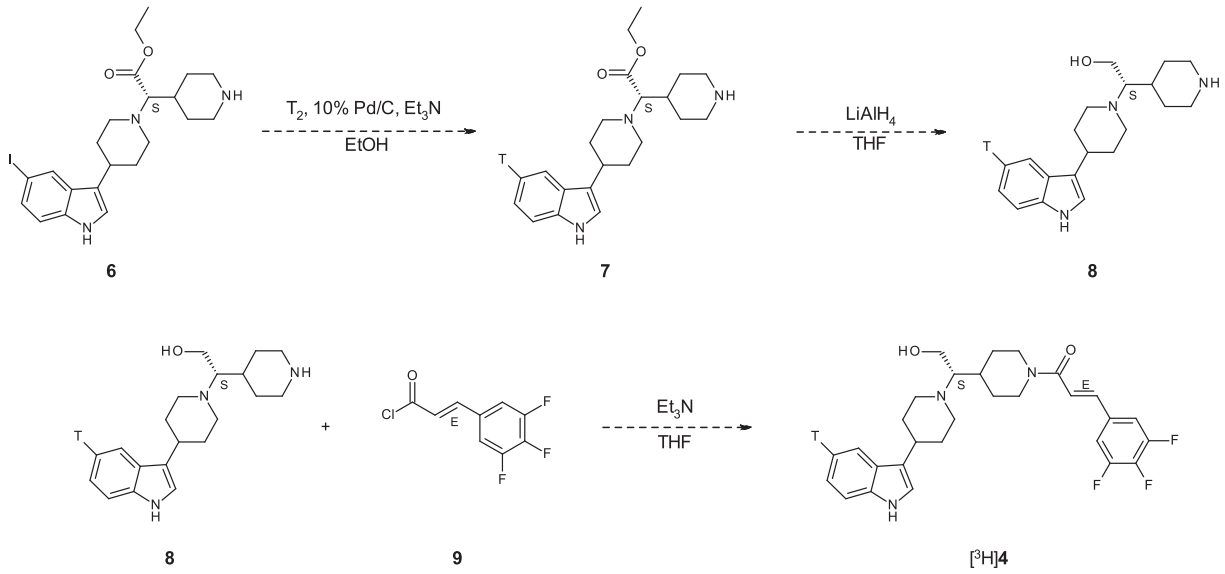

SCHEME 2 Envisioned synthesis sequence from **6** to [^{3}H]**4**. This route was first tried with deuterium, successfully yielding crude **4**-d_1

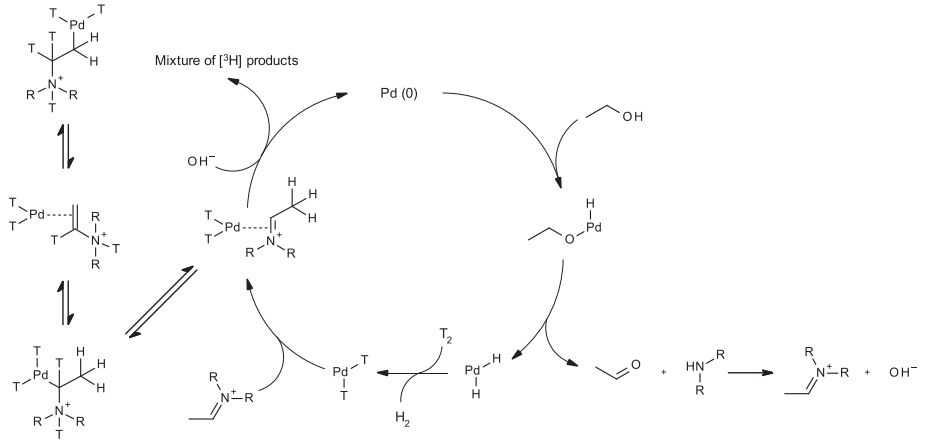

FIGURE 2 Proposed mechanism adapted from Corma et al[57] for the formation of the iminium ion species, which may then undergo double-bond migration prior to reduction in the presence of $^{3}H(g)$ and 10% Pd/C, yielding the mixture of radioactive compounds displayed in Figure 3

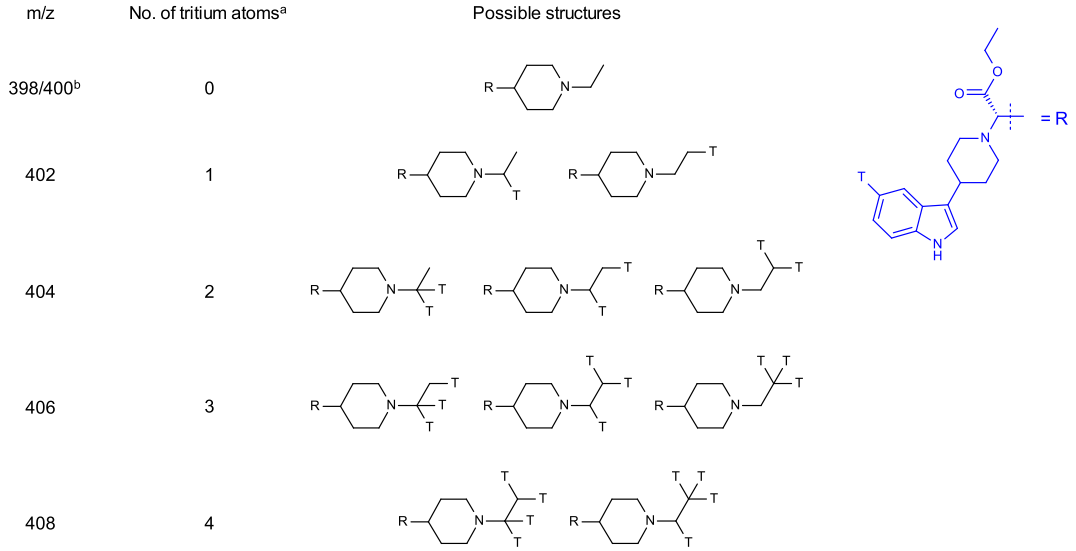

FIGURE 3 Mixture of products obtained from the observed side reaction with the *m/z* peaks on the mass spectrum corresponding to the respective number of tritium atoms incorporated into the structure. [a]This refers to the number of tritium atoms on the ethyl side chain and does not include the R part. [b]The *m/z* value of 398 corresponds to the nonradioactive compound where R also contains no tritium

Alternatively, Pd(II) could have been irreversibly reduced at a later, anaerobic stage. Moreover, the addition of alcohols to amines, *via* oxidation followed by a reductive amination, has been reported using a range of catalysts, including ruthenium[55] and more importantly palladium.[56,57] The mechanism of "chain walking", first introduced by Möhring et al,[58] is a process involving β-hydride elimination usually followed by immediate reinsertion, thus altering the regio-chemistry observed.[59] Its relevance in the context of this side reaction is that it could explain the mixture of products observed. Importantly, Culf et al have previously reported that such double-bond-migration processes can yield products of uncertain tritium distribution when using 10% Pd/C to reduce an alkene in methanol.[60] Furthermore, there is debate about the precise mechanism involved in the amination of alcohols in the presence of palladium catalysts, and it is possible that an intermolecular transfer hydrogenation from another amine takes place in the process,[61] contributing to the range of products observed.

The pattern in the mass spectrum and the ratio of integrals in the ^{3}H NMR spectrum can be rationalised by considering the incorporation of several ^{3}H atoms as outlined in Figure 3. Both non-aromatic ^{3}H peaks in the spectrum were broadened, which is in line with the different isotopic shifts of the possible species. The integral ratio between the two aliphatic peaks at 2.58 and 1.14 ppm in CD_3OD was approximately 1:1.33, slightly below the

1:1.5 that would be expected if incorporation at the $-CH_3$ vs the $-CH_2-$ position was completely random (Figure 3).

The second, and much more minor, side product can be explained in a similar fashion. During the lyophilisation process, ethanol was evaporated, followed by the addition of methanol and evaporation under nitrogen flow, which was repeated twice before passing a suspension in methanol through a syringe filter. It appears that during this process, a small amount of methanal was formed, which led to the *N*-methylated product in a similar manner as before. The ^{3}H NMR spectrum only shows one aliphatic peak at 2.33 (CD_3OD) as expected, and the observed mass distribution corresponds to 0, 1, 2, or 3 tritium atoms being incorporated on the methyl group. On the basis of these investigations, we attempted to use a different solvent, which would not be able to react with the secondary amine. Acetonitrile was chosen, and, as expected, neither of the two previous side products could be detected. However, the conversion was inefficient with only 700 MBq measured for the crude reaction mixture and 200 MBq after purification through preparative HPLC, with a theoretical radiochemical yield of 5.1 GBq. The $LiAlH_4$ reduction was attempted on the purified intermediate, yet the yield was again very low and insufficient to carry on further. This may be due to the fact that some of the desired products seemed to stick to the aluminium salts formed. Thus, it appeared that a change in solvent would not remedy the problem.

Hence, we decided to try the direct path to [^{3}H]**4**, to investigate whether short reaction times and low tritium pressure would be sufficient to keep the alkene functionality intact. To this end, we synthesised another batch of **4**, to prepare an iodinated precursor for radiolabelling.

The indole moiety of **4** was iodinated in an analogous manner before using *N*-iodosuccinimide (NIS) and trifluoroacetic acid (TFA) in dichloromethane (DCM), yielding compound **10**. When the reaction was tried with deuterium at a pressure of approximately 50 mbar and reaction times of both 15 minutes and 1 hour, fortunately, conversion to the desired product was achieved without affecting the C=C double bond. Hence, this reaction was carried out with tritium as shown in Scheme 3, successfully yielding [^{3}H]**4**.

2.4 | Autoradiography

With the radioligand in hand, it was possible to perform *in vitro* ARG studies on fresh frozen human brain slices to establish whether specific binding takes place in PD tissue. In addition to the PD sample, an MSA case, 2 AD cases (AD1 and AD2), and a control was examined (demographics are shown in Table 1).

As shown in Figure 4, in all cases the binding of [^{3}H]**4** at both 1 and 3 nM of concentration was not blocked by excess of unlabelled **4** compound (10 μM), suggesting a nonspecific binding of the radioligand (ie, to cell membranes and other high-capacity binding sites). One explanation for this result could be the relatively high log*P* value of around 4 leading to presence of the antagonist

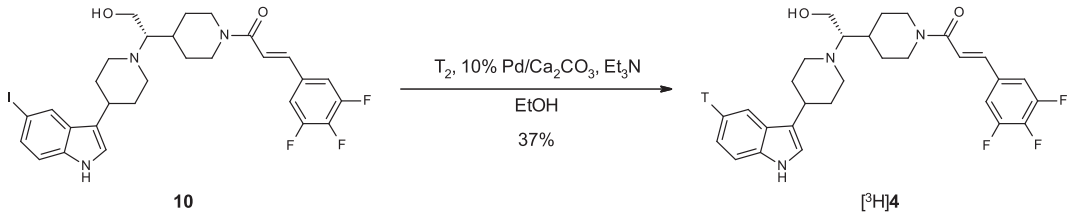

10 [^{3}H]**4**

SCHEME 3 The successful radio-synthesis of [^{3}H]**4**, using 10% Pd/Ca_2CO_3, a low tritium pressure of approximately 50 mbar, and a reaction time of 1 h to keep the alkene functionality intact

TABLE 1 Demographics of the human brain tissue from the Netherlands Brain Bank included in this study for the autoradiography experiment

Sample	Diagnosis	Brain Region	Age, y	Gender	PMD
PD	Parkinson's disease	Cingulate gyrus	82	M	06:05
MSA	Multiple system atrophy	Cerebellum	69	F	04:30
CT	Control	Cingulate gyrus	60	F	07:30
AD1	Alzheimer's disease	Frontal cortex	88	F	05:35
AD2	Alzheimer's disease	Frontal cortex	90	F	20:50

Note. Includes the sample, diagnosis, brain region, age (y), gender (M/F), and PMD.

Abbreviations: MSA, multiple-system atrophy; PMD, post-mortem delay.

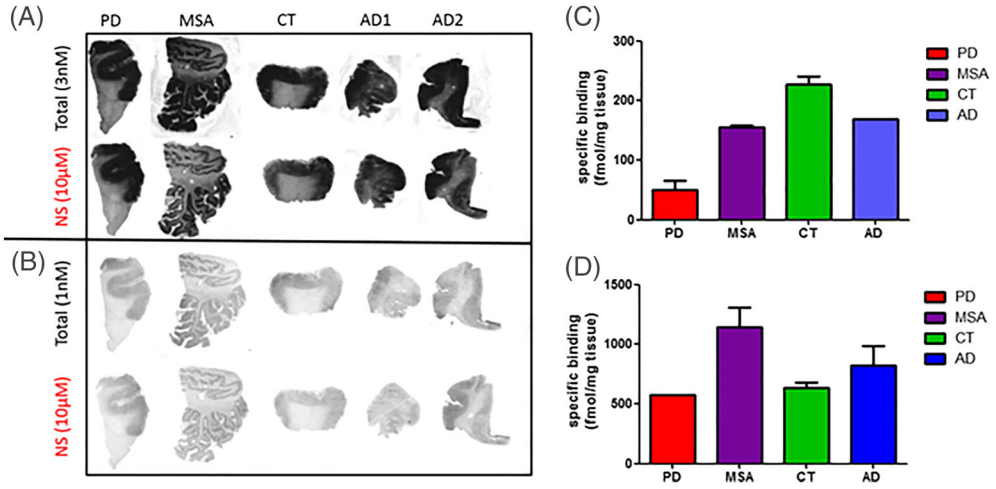

FIGURE 4 Autoradiograms showing [^{3}H]**4** total and nonspecific (NS) binding at 3 nM (A) and 1 nM (B) in human brain sections from a Parkinson's disease case (PD), a multiple-system atrophy (MSA) case, a nondemented control (CT), and a couple of Alzheimer's disease cases (AD1 and AD2). Displacement experiments with **4** (10 μM) did not show significant blocking, indicating low specific binding levels regardless of whether a 1 (**C**) or 3 nM (**D**) of concentration was used

in lipid tissue. Another possible reason could be the ubiquitous expression of CCR2. Thus, more experiments are currently ongoing in order to develop a less lipophilic and more specific radioligand for CCR2.

3 | CONCLUSION

In summary, CCR2 was envisioned as a potential target for ARG and eventually PET studies on neurodegenerative diseases. Based on previous development efforts, a promising small molecule antagonist (**4**) was selected and synthesised, and its binding affinity was confirmed. The initial attempt to create a tritium-labelled analogue of **4** *via* intermediate **5** gave rise to an interesting and unique side reaction profile. The use of Pd/C in ethanol as well as other alcohols is very common not only for tritium labelling reactions but also in organic chemistry in general. Therefore, we believe that this work can act as a cautionary tale to other chemists, in particular radiochemists, who may encounter this type of side reaction. This would be especially relevant to anyone working with compounds featuring amines that could be subject to this type of alkylation. After, eventually, preparing [^{3}H]**4** and learning that direct labelling presented a simpler solution than initially thought, the radioligand was used for *in vitro* ARG measurements on human brain slices. Unfortunately, the total binding obtained was not blocked by an excess of the nonlabelled "cold" compound (10 μM), suggesting that most of the signal corresponds to nonspecific binding. Thus, further work is needed to establish whether CCR2 antagonists are viable in this context or whether the ubiquitous expression of this receptor generally precludes any impactful measurements.

4 | EXPERIMENTAL SECTION

4.1 | General

All chemicals were purchased from Combi Blocks, Sigma-Aldrich, or its subsidiaries. Tritium was obtained from RC Tritec AG. Anhydrous solvents were obtained from Aldrich and were used without further purification. Reactions were magnetically stirred unless otherwise noted. Tritium reactions were performed on an RC Tritec Tritium manifold.

^{1}H NMR and ^{13}C NMR spectra were acquired on a Bruker Avance III spectrometer running at a proton frequency of 500.1 MHz and fitted with a cryogenic probe or on Bruker Avance Nanobay spectrometers operating at 400 MHz. Chemical shifts are reported in ppm (δ) relative to tetramethylsilane (TMS) with the solvent resonance as internal standard (5.32 and 53.84 ppm for CD_2Cl_2, 7.26 and 77.16 ppm for $CDCl_3$, 3.31 and 49.00 ppm for CD_3OD, and 2.50 and 39.52 ppm for DMSO-d_6).[62] The signals derived from the ^{1}H NMR spectra are reported with chemical shifts, multiplicity (s = singlet, d = doublet, t = triplet, q = quartet, p = pentet, sxt = sextet, dt = doublet of triplets, dq = doublet of quartets, ddd = double doublet of doublets, ddt = double doublet of triplets, td = triplet of doublets, tt = triplet of triplets, qd = quartet of doublets, or m = multiplet), coupling constant (Hz), and integration. Data for ^{13}C NMR are reported with

chemical shifts and coupling to ^{19}F, where observed. Flash column chromatography was carried out using pre-packed silica gel columns supplied by Biotage and using a Biotage automated flash systems with UV detection.

HPLC was performed using a system composed of a Gilson 322 Pump equipped with a Gilson UV/VIS-152 detector with an Xbridge Prep C-18 10 μm OBD 19 × 250 mm column. Separation of enantiomers was performed on a Nova SuperSep150 and analysed by Waters Acquity UPC^2. In the radioactive reaction sequence, HPLC was performed using a system composed of a Gilson 322 Pump equipped with a Gilson Ready 2000 detector with an XbridgeTM Prep C-18 5 μm OBDTM 19 × 100 mm column.

LCMS were acquired on a Waters Acquity UPLC using a BEH C18 column (50 mm × 2.1 mm, 1.7-μm particles) with a gradient of 10% to 90% over 4 min with MeCN–NH_4/NH_4CO_3 or MeCN–formic acid and electrospray ionisation.

4.2 | Precursor synthesis

4.2.1 | *tert*-Butyl 4-(1-bromo-2-ethoxy-2-oxoethyl) piperidine-1-carboxylate (11)

An oven-dried, two-neck, round-bottom flask equipped with a dropping funnel was flushed with nitrogen and cooled to −78°C. Lithium bis(trimethylsilyl)amide in THF (1M, 100 mL, 100 mmol) was added, followed by *tert*-butyl 4-(2-ethoxy-2-oxoethyl)piperidine-1-carboxylate (15.1 g, 55.5 mmol) in dry THF (55 mL). The orange solution was stirred at −78°C for 3 hours under a blanket of N_2. Then chlorotrimethylsilane (12.69 mL, 100 mmol) was added dropwise at −78°C, and the mixture was stirred for another hour. Subsequently, dibromine (3.44 mL, 66.6 mmol) was added dropwise, and the dropping funnel was then washed with a little dry THF (approximately 5 mL). The mixture was stirred for another 2 hours; then it was warmed to 0°C and stirred for another hour under N_2. The mixture was diluted with ethyl acetate (approximately 200 mL) and washed with sat. $NaHCO_3$ solution (120 mL) and then with water (150 mL). The organic phases were dried over a phase separator cartridge and concentrated under reduced pressure to afford a yellow oil. The residue was purified by passing it through a Biotage samplet cartridge (Biotage SNAP Samplet KP-SIL 34 g, 6/cs), washing with a 50:50 ethyl acetate:*n*-heptane mixture. Note: This rapid purification step was chosen since it appeared as if the product degraded over time. The solvent was removed on the rotary evaporator. A yellow oil, *tert*-butyl 4-(1-bromo-2-ethoxy-2-oxoethyl)piperidine-1-carboxylate (**11**) (22.0 g, approximately 50% pure by UV), was obtained that was used directly in the next step.

LC/MS (M + 1): 350.2 (82%), 352.2 (100%).

^{13}C NMR (101 MHz, CD_3Cl): δ (ppm) 168.9, 154.5, 79.5, 61.9, 51.6, 49.1, 39.8, 28.4, 22.7, 14.0.

4.2.2 | *tert*-Butyl (*S*)-4-(1-(4-(1*H*-indol-3-yl) piperidin-1-yl)-2-ethoxy-2-oxoethyl)piperidine-1-carboxylate (5)

Under air, crude *tert*-butyl 4-(1-bromo-2-ethoxy-2-oxoethyl)piperidine-1-carboxylate (**11**) (11.0 g, 31.41 mmol) (the actual amount of reactant is not truly known as it was used directly without thorough purification to avoid degradation), 3-(piperidin-4-yl)-1*H*-indole (10.1 g, 50.25 mmol), and triethylamine (8.75 mL, 62.81 mmol) were combined in MeCN (80 mL) and refluxed overnight. The solvent was removed on the rotavapor, and the orange/brown solid was purified *via* automated flash column chromatography (98:2 → 80:20, DCM:MeOH; 340 g of SNAP column) to afford an orange oil. This was then further purified again *via* automated flash column chromatography (88:12 → 0:100, *n*-heptane:ethyl acetate), to afford *tert*-butyl 4-(1-(4-(1*H*-indol-3-yl)piperidin-1-yl)-2-ethoxy-2-oxoethyl)piperidine-1-carboxylate (3.25 g) as an off-white solid. This racemate was separated by chiral SFC (25% EtOH/DEA 100/0.5 in CO_2, 120 bar, 40°C, CelluCoat 5 μM 250 × 30 mm column, 100 mL/min), which afforded *tert*-butyl (*R*)-4-(1-(4-(1*H*-indol-3-yl)piperidin-1-yl)-2-ethoxy-2-oxoethyl)piperidine-1-carboxylate (1.39 g, 2.95 mmol) and *tert*-butyl (*S*)-4-(1-(4-(1*H*-indol-3-yl)piperidin-1-yl)-2-ethoxy-2-oxoethyl)piperidine-1-carboxylate (**5**) (1.39 g, 2.95 mmol, 9.5%) as off-white solids.

LC/MS (M + 1): 470.5 (100%).

^1H NMR (400 MHz, CD_2Cl_2): δ (ppm) 8.28 (s, 1H), 7.61 (d, J = 7.9 Hz, 1H), 7.35 (d, J = 8.0 Hz, 1H), 7.15 (t, J = 7.5 Hz, 1H), 7.06 (t, J = 7.4 Hz, 1H), 6.98 (s, 1H), 4.21 (tt, J = 12.3, 5.4 Hz, 2H), 4.02 to 4.14 (m, 2H), 2.67 to 3.02 (m, 6H), 2.60 (t, J = 10.8 Hz, 1H), 2.34 (t, J = 11.1 Hz, 1H), 1.92 to 2.06 (m, 4H), 1.80 (td, J = 12.3, 12.2, 3.7 Hz, 1H), 1.67 (dd, J = 12.3, 3.2 Hz, 1H), 1.48 to 1.54 (m, 1H), 1.45 (s, 9H), 1.31 (d, J = 7.1 Hz, 3H), 1.13 (ddt, J = 17.4, 11.6, 5.0 Hz, 2H).

^{13}C NMR (101 MHz, CD_2Cl_2): δ (ppm) 171.1, 155.1, 136.9, 127.1, 122.1, 121.8, 120.1, 119.4, 119.2, 111.5, 79.4, 73.2, 60.2, 47.3, 44.9, 44.4, 35.1, 34.3, 34.2, 34.0, 29.9, 29.3, 28.6, 27.1, 14.9.

tert-Butyl (*R*)-4-(1-(4-(1*H*-indol-3-yl)piperidin-1-yl)-2-ethoxy-2-oxoethyl)piperidine-1-carboxylate.

$[\alpha]^{20}_D$ + 35° (c = 1.0, acetonitrile).

tert-Butyl (*S*)-4-(1-(4-(1*H*-indol-3-yl)piperidin-1-yl)-2-ethoxy-2-oxoethyl)piperidine-1-carboxylate (**5**).

$[\alpha]^{20}_{D} - 36°$ ($c = 1.0$, acetonitrile).

4.2.3 | *tert*-Butyl (*S*)-4-(1-(4-(1*H*-indol-3-yl) piperidin-1-yl)-2-hydroxyethyl)piperidine-1-carboxylate (12)

An oven-dried, round-bottom flask was evacuated and backfilled with nitrogen three times. It was cooled to 0°C, and lithium aluminium hydride in THF (1M, 958 μL, 0.96 mmol) was added, followed by dropwise addition of *tert*-butyl 4-(1-(4-(1*H*-indol-3-yl)piperidin-1-yl)-2-ethoxy-2-oxoethyl)piperidine-1-carboxylate (**5**) (300 mg, 0.64 mmol) in dry THF (18 mL) under N_2. The mixture was stirred at 0°C for 1 hour before being allowed to warm to room temperature (RT). After being stirred for another hour at RT, water (40 μL) was slowly added to quench, followed by 4M NaOH (40 μL) and, once again, water (120 μL). The mixture was stirred for 30 minutes and then filtered through a celite pad to remove the solids, and the layers were separated. The aqueous phase was washed twice with ethyl acetate. The organic layers were combined, washed with brine, and dried over a phase separator cartridge. The solvent was removed on the rotary evaporator to afford *tert*-butyl (*S*)-4-(1-(4-(1*H*-indol-3-yl)piperidin-1-yl)-2-hydroxyethyl)piperidine-1-carboxylate (**12**) (270 mg, 99%) as a yellow solid.

LC/MS (M + 1): 428.4 (100%).

^{1}H NMR (400 MHz, CD_3Cl): δ (ppm) 8.25 (s, 1H), 7.63 (d, $J = 7.9$ Hz, 1H), 7.35 (d, $J = 8.1$ Hz, 1H), 7.18 (t, $J = 7.5$ Hz, 1H), 7.10 (t, $J = 7.4$ Hz, 1H), 6.95 (d, $J = 1.8$ Hz, 1H), 3.58 (dd, $J = 9.5$, 4.5 Hz, 1H), 3.28 (td, $J = 10.2$, 7.5 Hz, 1H), 3.03 to 3.16 (m, 1H), 2.82 to 3.01 (m, 4H), 2.69 (d, $J = 14.9$ Hz, 1H), 2.60 (ddd, $J = 15.2$, 8.7, 4.8 Hz, 1H), 2.43 to 2.56 (m, 1H), 2.27 (s, 1H), 2.08 (d, $J = 6.4$ Hz, 2H), 1.85 to 1.95 (m, 2H), 1.59 to 1.82 (m, 3H), 1.53 (td, $J = 12.2$, 3.5 Hz, 1H), 1.48 (s, 9H), 1.44 (s, 1H), 1.27 to 1.4 (m, 2H).

^{13}C NMR (101 MHz, CD_3Cl): δ (ppm) 171.3, 154.9, 136.5, 126.7, 126.6, 125.62, 122.0, 122.0, 121.4, 121.3, 119.8, 119.2, 119.1, 119.1, 111.4, 79.6, 69.7, 69.6, 60.5, 58.6, 58.5, 55.8, 55.8, 55.1, 54.9, 46.5, 45.2, 44.9, 36.2, 35.3, 34.7, 34.7, 34.1, 34.1, 34.0, 34.0, 32.1, 31.7, 30.4, 29.0, 28.9, 28.6, 21.2, 14.3.

4.2.4 | (*S*)-2-(4-(1*H*-indol-3-yl)piperidin-1-yl)-2-(piperidin-4-yl)ethan-1-ol (13)

To *tert*-butyl (*S*)-4-(1-(4-(1*H*-indol-3-yl)piperidin-1-yl)-2-hydroxyethyl)piperidine-1-carboxylate (**12**) (35 mg, 0.08 mmol) in DCM (15 mL) was added hydrogen chloride in diethyl ether (2.0 M, 409 μL, 0.82 mmol) at RT under air. A sudden colour change from yellow to orange was observed, and red precipitate was formed. The mixture was stirred at RT overnight. The solvent was removed on the rotavapor; and the orange solid, (*S*)-2-(4-(1*H*-indol-3-yl)piperidin-1-yl)-2-(piperidin-4-yl) ethan-1-ol (**13**) (27 mg, 0.07 mmol, 91%), was used in the next step without further purification.

LC/MS (M + 1): 328.4 (100%), 329.4 (21%).

4.2.5 | (*E*)-3-(3,4,5-Trifluorophenyl) acryloyl chloride (9)

(*E*)-3-(3,4,5-Trifluorophenyl)acrylic acid (500 mg, 2.47 mmol) was dissolved in DCM (15 mL), and two drops of dimethylformamide (DMF) were added. Oxalyl dichloride (419 μL, 4.95 mmol) was slowly added at RT. The clear solution was stirred at RT under air for 2 hours. The resulting mixture was concentrated under reduced pressure to afford (*E*)-3-(3,4,5-trifluorophenyl)acryloyl chloride (**9**) (540 mg, 2.45 mmol, 99%) as a yellow oil in quantitative yield, which was used directly in the next step.

^{1}H NMR (400 MHz, CD_3Cl): δ (ppm) 7.65 (d, $J = 15.6$ Hz, 1H), 7.21 (dd, $J = 7.6$, 6.6 Hz, 2H), 6.56 (d, $J = 15.6$ Hz, 1H).

^{13}C NMR (101 MHz, CD_3Cl): δ (ppm) 166.3, 166.2, 165.6, 164.0, 147.2, 146.8, 124.9, 124.8, 113.3, 113.2, 113.0, 105.1.

4.2.6 | (*S*,*E*)-1-(4-(1-(4-(1*H*-Indol-3-yl) piperidin-1-yl)-2-hydroxyethyl)piperidin-1-yl)-3-(3,4,5-trifluorophenyl)prop-2-en-1-one (4)

2-(4-(1*H*-Indol-3-yl)piperidin-1-yl)-2-(piperidin-4-yl)ethan -1-ol (**13**) (26 mg, 0.08 mmol) and (*E*)-3-(3,4,5-tri fluorophenyl)acryloyl chloride (**9**) (17.51 mg, 0.08 mmol) were combined in dry THF (6 mL) followed by a few drops of triethylamine (11.07 μL, 0.08 mmol) under air. The mixture was stirred at RT for 5 hours. The solid residue was purified *via* HPLC (30-90% MeCN–0.2% NH_4OH over 25 min, XbridgeTM Prep C-18 10 μm OBDTM 19 × 250 mm column, 20 mL/min). The solvent was removed under reduced pressure to afford a white solid, (*S*,*E*)-1-(4-(1-(4-(1*H*-indol-3-yl)piperidin-1-yl)-2-hydroxye thyl)piperidin-1-yl)-3-(3,4,5-trifluorophenyl)prop-2-en-1-one (**4**) (22.0 mg, 54.2%).

LC/MS (M + 1): 512.3 (100%), 513.3 (31%), 514.3 (3%).

^{1}H NMR (400 MHz, CD_3Cl): δ (ppm) 8.05 (s, 1H), 7.62 (d, $J = 7.0$ Hz, 1H), 7.49 (d, $J = 15.3$ Hz, 1H), 7.37 (d, $J = 7.9$ Hz, 1H), 7.19 (t, $J = 7.3$ Hz, 1H), 7.09 to 7.16 (m, 3H), 6.97 (s, 1H), 6.82 (d, $J = 15.1$ Hz, 1H), 4.75 (s,

1H), 4.10 (s, 1H), 3.59 (s, 1H), 3.49 (s, 1H), 3.25 to 3.39 (m, 1H), 3.03 to 3.22 (m, 2H), 2.85 to 3.01 (m, 3H), 2.59 to 2.74 (m, 2H), 2.50 (s, 1H), 2.06 to 2.15 (m, 3H), 1.94 (d, J = 8.3 Hz, 1H), 1.63 to 1.86 (m, 3H), 1.35 to 1.49 (m, 1H), 1.19 to 1.28 (m, 1H).

^{13}C NMR (101 MHz, CD_3Cl): δ (ppm) 164.4, 152.8, 152.7, 150.3, 139.6, 136.5, 131.7, 126.7, 122.2, 121.3, 119.8, 119.8, 119.3, 119.1, 111.8, 111.8, 111.6, 111.4, 69.5, 58.6, 54.6, 54.6, 51.0, 46.2, 45.8, 45.4, 42.6, 36.4, 36.2, 34.6, 34.1, 33.9, 32.7, 31.5, 29.9, 28.8.

4.3 | Iodination

4.3.1 | (*S*)-2-(4-(5-Iodo-1*H*-indol-3-yl) piperidin-1-yl)-2-(piperidin-4-yl)ethan-1-ol (14) (failed)

Under air, *tert*-butyl (*S*)-4-(1-(4-(1*H*-indol-3-yl)piperidin-1-yl)-2-hydroxyethyl)piperidine-1-carboxylate (**13**) (127 mg, 0.30 mmol) and NIS (80 mg, 0.36 mmol) were combined in DCM/TFA (1:1 v/v, 3 mL). The solution quickly turned dark red/purple and was stirred at RT overnight. The dark solution was dried under nitrogen flow. The solid residue was further purified *via* HPLC (20-95% MeCN–0.1% TFA over 25 min, XbridgeTM Prep C-18 10 μm OBDTM 19 × 250 mm column, 20 mL/min), which afforded a mixture of regio-isomers that could unfortunately not be successfully separated.

Note: Attempts to separate these were to no avail, since the compound was not stable on the HPLC column at pH 10, coelution occurred at pH 3, and it appeared to degrade upon storage in DMSO.

LC/MS (M + 1) of isomeric mixture: 454.2 (100%).

4.3.2 | Ethyl (*S*)-2-(4-(5-iodo-1*H*-indol-3-yl) piperidin-1-yl)-2-(piperidin-4-yl)acetate (6)

Under air, *tert*-butyl (*S*)-4-(1-(4-(1*H*-indol-3-yl)piperidin-1-yl)-2-ethoxy-2-oxoethyl)piperidine-1-carboxylate (**5**) (84 mg, 0.18 mmol) and NIS (48.3 mg, 0.21 mmol) were combined in DCM/TFA (1:1 v/v, 3 mL). The solution quickly turned dark red/purple and was stirred at RT overnight. The dark solution was dried under nitrogen flow. The solid residue was further purified *via* preparative HPLC (20-80% MeCN–0.1% TFA over 25 min, XbridgeTM Prep C-18 10 μm OBDTM 19 × 250 mm column, 20 mL/min). The solvent was removed on the rotavapor, and the isomers were separated *via* SFC ($MeOH/H_2O/NH_3$ 97/3/50 mM, Waters Prep 100 SFC MS with a Waters BEH 5 μm 30 × 250 mm column) ethyl (*S*)-2-(4-(5-iodo-1*H*-indol-3-yl)piperidin-1-yl)-2-(piperidin-4-yl)acetate (**6**) (12.0 mg, 13.54%) was obtained as an off-white solid.

LC/MS (M + 1): 496.2 (100%), 497.2 (24%).

^{1}H NMR (400 MHz, CD_3Cl): δ (ppm) 8.02 (s, 1H), 7.94 (d, J = 1.4 Hz, 1H), 7.42 (dd, J = 8.5, 1.6 Hz, 1H), 7.13 (d, J = 8.5 Hz, 1H), 6.92 (s, 1H), 4.17 to 4.27 (m, 2H), 3.11 to 3.25 (m, 2H), 2.96 (d, J = 10.4 Hz, 2H), 2.87 (d, J = 11.5 Hz, 1H), 2.52 to 2.76 (m, 4H), 2.25 to 2.37 (m, 1H), 1.99 (d, J = 13.2 Hz, 5H), 1.76 (td, J = 12.4, 12.3, 3.8 Hz, 1H), 1.55 to 1.64 (m, 2H), 1.21 to 1.37 (m, 5H).

^{13}C NMR (101 MHz, CD_3Cl): δ (ppm) 171.1, 171.0, 135.5, 130.3, 129.5, 128.2, 121.3, 120.5, 113.3, 82.7, 73.0, 60.1, 54.1, 47.0, 46.1, 45.8, 34.5, 33.9, 33.8, 33.6, 29.9, 29.3, 14.9.

4.3.3 | (*S*,*E*)-1-(4-(2-Hydroxy-1-(4-(5-iodo-1*H*-indol-3-yl)piperidin-1-yl)ethyl) piperidin-1-yl)-3-(3,4,5-trifluorophenyl) prop-2-en-1-one (10)

Under air, (*S*,*E*)-1-(4-(1-(4-(1*H*-indol-3-yl)piperidin-1-yl)-2-hydroxyethyl)piperidin-1-yl)-3-(3,4,5-trifluorophenyl) prop-2-en-1-one (**4**) (20 mg, 0.04 mmol) and NIS (11.43 mg, 0.05 mmol) were combined in DCM/TFA (3:1 v/v, 2 mL) and stirred overnight at RT. The solvent was removed on the rotavapor, and the light brown residue was purified *via* preparative HPLC (20-80% MeCN–0.1% TFA over 30 min, XbridgeTM Prep C-18 10 μm OBDTM 19 × 250 mm column, 20 mL/min) to afford a beige solid, (*S*,*E*)-1-(4-(2-hydroxy-1-(4-(5-iodo-1*H*-indol-3-yl)piperidin-1-yl)ethyl)piperidin-1-yl)-3-(3,4,5-trifluorophenyl)prop-2-en-1-one (**10**) (17.0 mg, 68.2%).

LC/MS (M + 1): 638.2 (100%).

4.4 | Deuterium trial reaction

4.4.1 | Ethyl (*S*)-2-(4-(1*H*-indol-3-yl) piperidin-1-yl)-2-(piperidin-4-yl)acetate-d_1 (15)

Ethyl 2-(4-(5-iodo-1*H*-indol-3-yl)piperidin-1-yl)-2-(piperidin-4-yl)acetate (**6**) (2 mg, 4.04 μmol), palladium on activated charcoal (2 mg, 0.02 mmol), and triethylamine (40 μL, 4.04 μmol) were combined in ethanol (0.5 mL). The mixture was frozen in liquid nitrogen, and the flask was evacuated before closing the vacuum tap and being allowed to warm to RT. This was performed twice. Then the mixture was frozen once more, and deuterium gas was pulled into the flask (which was still under vacuum; ie, the tap was closed). The mixture was allowed to warm to RT and stirred for 4 hours. The suspension was diluted with ethanol (5 mL) and filtered through a phase separator cartridge, and the solvent removed on the rotovap.

The product was afforded as a yellow solid that was used directly in the next step.

LC/MS (M + 1): 371.3 (100%).

4.4.2 | (*S*)-2-(4-(1*H*-Indol-3-yl)piperidin-1-yl)-2-(piperidin-4-yl)ethan-1-ol-d_1 (16)

An oven-dried, round-bottom flask was evacuated and backfilled with nitrogen three times. To it was added lithium aluminium hydride (0.22 mL, 0.22 mmol) in THF (1M), and it was then cooled to 0°C. Another flask containing ethyl 2-(4-(1*H*-indol-3-yl-5-*d*)piperidin-1-yl)-2-(piperidin-4-yl)acetate-d_1 (2 mg, 5.40 μmol) was evacuated and backfilled with nitrogen three times before adding anhydrous THF (3 mL). The yellow solution was added slowly to the $LiAlH_4$ under N_2. The mixture was stirred at 0°C for 1 hour before being allowed to warm to RT. It was stirred for another 1.5 hours at RT. Water (0.5 mL) was slowly added to quench, followed by 4M of NaOH (1 mL) and water (0.5 mL). The mixture was filtered over a syringe filter and dried over a phase separator cartridge, and the aqueous phase was washed twice with ethyl acetate (still on the phase separator). The solvent was removed on the rotary evaporator to yield a solid.

LC/MS (M + 1): 329.2 (100%).

4.4.3 | (*S*,*E*)-1-(4-(1-(4-(1*H*-Indol-3-yl) piperidin-1-yl)-2-hydroxyethyl)piperidin-1-yl)-3-(3,4,5-trifluorophenyl)prop-2-en-1-one (4-d_1)

To 2-(4-(1*H*-indol-3-yl-5-*d*)piperidin-1-yl)-2-(piperidin-4-yl)ethan-1-ol (**16**) (1.5 mg, 4.57 μmol) was added (*E*)-3-(3,4,5-trifluorophenyl)acryloyl chloride (**9**) (4 mg, 0.02 mmol), and the flask was evacuated and backfilled with nitrogen three times. Then dry THF (3 mL) followed by a few drops of triethylamine (0.637 μL, 4.57 μmol) was added under N_2. The mixture was stirred at RT for 3 hours; then the solvent was removed on the rotovap. LCMS indicated formation of (*S*,*E*)-1-(4-(1-(4-(1*H*-indol-3-yl)piperidin-1-yl)-2-hydroxyethyl) piperidin-1-yl)-3-(3,4,5-trifluorophenyl) prop-2-en-1-one (**4**-d_1).

LC/MS (M + 1): 513.3 (100%).

4.5 | Radiochemistry—synthesis

4.5.1 | [^{3}H] ethyl (*S*)-2-(4-(1*H*-indol-3-yl) piperidin-1-yl)-2-(piperidin-4-yl)acetate (7)

Approach 1

Ethyl (*S*)-2-(4-(5-iodo-1*H*-indol-3-yl)piperidin-1-yl)-2-(piperidin-4-yl)acetate (**6**) (2.4 mg, 4.84 μmol), palladium on activated charcoal (2.2 mg, 0.02 mmol), and triethylamine (40 μL, 4.84 μmol) were combined in ethanol (0.5 mL). The mixture was frozen in liquid nitrogen, and the flask evacuated before closing the vacuum tap and being allowed to warm to RT. This was performed twice. The mixture was frozen once more and the flask evacuated; then tritium was released from the uranium bed by heating it with a blowtorch. The reaction was run with a partial pressure of tritium gas (337.3 GBq) and was warmed to RT with stirring for 3 hours. The tritium gas in the flask was blown of together with the solvent under nitrogen flow. Then 0.5 mL of methanol was added and the solvent evaporated as before. This was performed twice. It was taken up in methanol once more and then passed through a syringe filter, and the solvent was evaporated under reduced pressure to yield a solid (2.5 GBq), which was purified *via* preparative HPLC (10-80% MeCN–0.2% NH_3OH over 30 min, Xbridge Prep C-18 5 μm OBD 19 × 100 mm column, 10 mL/min).

[^{3}H] ethyl (*S*)-2-(4-(1*H*-indol-3-yl)piperidin-1-yl)-2-(1-ethylpiperidin-4-yl)acetate (**17**):

LC/MS (M + 1): 398.3 (27%), 400.3 (100%), 402.3 (98%), 404.3 (44%), 406.3 (28%), 408.3 (11%), 410.3 (1%).

^{3}H NMR (533 MHz, CD_3OD): δ (ppm) 7.04 (t, J = 7.8 Hz), 2.58 (b), 1.14 (b).

[^{3}H] ethyl (*S*)-2-(4-(1*H*-indol-3-yl)piperidin-1-yl)-2-(1-methylpiperidin-4-yl)acetate (**18**).

LC/MS (M + 1): 384.2 (26%), 386.2 (100%), 488.3 (74%), 490.3 (3%).

^{3}H NMR (533 MHz, CD_3OD): δ (ppm) 7.04 (t, J = 7.7 Hz), 2.33 (b).

Approach 2

Ethyl 2-(4-(5-iodo-1*H*-indol-3-yl)piperidin-1-yl)-2-(piperidin-4-yl)acetate (**6**) (2.4 mg, 4.84 μmol), palladium on activated charcoal (2.2 mg, 0.02 mmol), and triethylamine (40 μL, 4.84 μmol) were combined in acetonitrile (0.7 mL). The mixture was frozen in liquid nitrogen, and the flask evacuated before closing the vacuum tap and being allowed to warm to RT. This was performed twice. The mixture was frozen once more and the flask evacuated; then tritium was released from the uranium bed by heating it with a blowtorch. The reaction was run with a partial pressure of tritium gas (336.4 GBq) and was warmed to RT with stirring for 3 hours. The tritium gas in the flask was blown of together with the solvent under nitrogen flow. Then 0.5 mL of acetonitrile was added and the solvent evaporated as before. This was performed twice. The mixture was then passed through a syringe filter, and the solvent was evaporated under a stream of nitrogen to yield a yellow solid, (approximately 700 MBq). This was purified by preparative HPLC (25-

75% MeCN–0.2% NH_3 over 35 min, Xbridge Prep C-18 5 μm OBD 19 × 100 mm column, 10 mL/min).

LC/MS (M + 1): 372.2 (100%), 373.2 (30%).

4.5.2 | [^{3}H] (*S*)-2-(4-(1*H*-Indol-3-yl) piperidin-1-yl)-2-(piperidin-4-yl)ethan-1-ol (8) (failed)

An oven-dried, round-bottom flask was evacuated and backfilled with nitrogen three times. It was charged with lithium aluminium hydride in THF (1M, 0.2 mL, 0.20 mmol) and cooled to 0°C. Another flask containing [^{3}H] ethyl (*S*)-2-(4-(1*H*-indol-3-yl)piperidin-1-yl)-2-(piperidin-4-yl)acetate (**7**) (200 MBq) was evacuated and backfilled with nitrogen before adding anhydrous THF (3 mL). The yellow solution containing [^{3}H] ethyl (*S*)-2-(4-(1*H*-indol-3-yl)piperidin-1-yl)-2-(piperidin-4-yl)acetate was slowly added to the $LiAlH_4$ solution under N_2. The mixture was stirred at 0°C for 1 hour before being allowed to warm to RT. It was stirred for another 2 hours at RT. The mixture was quenched with TFA (50 μL), the solvent evaporated under a stream of nitrogen, and the crude material purified *via* preparative HPLC (10-60% MeCN–0.1% TFA over 30 min, Xbridge Prep C-18 5 μm OBD 19 × 100 mm column, 10 mL/min). Unfortunately, the product could not be detected in any of the fractions or the reaction flask. Most active fraction contained approximately 40 MBq. It is possible that the product stuck to the aluminium salts and remained on the pre-column filter.

Crude LC/MS (M + 1): 330.2 (100%), 331.2 (11%).

4.5.3 | [^{3}H] (*S*,*E*)-1-(4-(1-(4-(1*H*-Indol-3-yl) piperidin-1-yl)-2-hydroxyethyl)piperidin-1-yl)-3-(3,4,5-trifluorophenyl)prop-2-en-1-one ([^{3}H]4)

(*S*,*E*)-1-(4-(2-Hydroxy-1-(4-(5-iodo-1*H*-indol-3-yl)piperidin-1-yl)ethyl)piperidin-1-yl)-3-(3,4,5-trifluorophenyl)prop-2-en-1-one (**10**) (0.6 mg, 0.94 μmol), palladium on calcium carbonate (1.944 mg, 0.94 μmol), and triethylamine (20 μL, 0.94 μmol) were combined in ethanol (0.6 mL). The mixture was frozen in liquid nitrogen, and the flask evacuated before closing the vacuum tap and being allowed to warm to RT. This was performed twice. The mixture was frozen once more and the flask evacuated; then tritium (50 mbar) was released from the uranium bed by heating it with a blowtorch. The mixture was warmed to RT and stirred for 1 hour. The tritium gas in the flask was blown off together with the solvent under nitrogen flow. Then 0.5 mL of methanol was added and the solvent evaporated as before. This was performed twice. The crude mixture was taken up in methanol once more and then passed through a syringe filter, and the solvent was evaporated under reduced pressure to yield a solid (approximately 500 MBq) that was purified *via* preparative HPLC (10-70% MeCN–0.1% TFA over 30 min, Xbridge Prep C-18 5 μm OBD 19 × 100 mm column, 10 mL/min). The radioactive purity of the residue (370 MBq, 0.9% radiochemical, and 37% chemical yield) was determined to be 96% by HPLC.

The isotopic incorporation was determined by mass spectrometry to be 16% unlabelled, 82% monolabelled, and 2% dilabelled to give a molar activity of 900 GBq/mmol.

Chemical purity: greater than 90%. Chiral purity: 99 ee.

HPLC analysis method: Waters Xbridge C18 3.5 μm, 4.6 × 100 mm column, −60°C. Eluent A: Water + 10 mM ammonium formate pH 3. Eluent B: MeCN, flow rate 0.6 mL/min, UV detection 254 nm, retention time 14.5 min. Gradient: 0 minute—5% B; 3 minutes—5% B; 25 minutes—95% B; 30 minutes—95% B.

LC/MS (M + 1): 514.3 (100%), 515.2 (37%), 516.3 (14%).

^{3}H NMR (533 MHz, CD_3OD): δ (ppm) 7.36 (d, J = 8.6 Hz), 7.09 to 7.14 (m), 7.02 (t, J = 8.0) (integral ratio 0.2:0.4:1.0).

4.6 | Autoradiography

Post-mortem brain tissues of different pathologies were obtained from the Netherlands Brain Bank and used for the *in vitro* ARG. The frozen sections were allowed to reach room temperature, pre-incubated for 15 minutes with binding buffer (50 mM Tris HCl 120 mM NaCl, 5 mM KCl, 2 mM $CaCl_2$, 1 mM $MgCl_2$, at pH 7.4), and then incubated for 1 hour at room temperature with the tritiated compound using different concentrations (3 and 1 nM). To determine the specific binding, adjacent sections were coincubated with the cold compound (unlabelled) at 10 μM. After incubation, the slides were washed three times in washing buffer (50 mM Tris HCl, pH 7.4) followed by a brief wash in distilled water. The slides were then dried and exposed to phosphor imaging plates (Fujifilm Plate BAS-TR2025, Fujifilm, Tokyo, Japan). Tritium microscale standards (American Radiolabeled Chemicals Inc) were placed in cassettes together with the sections for calibration and quantification of the binding density. The phosphor imaging plates, exposed for approximately 90 hours, were scanned, and the resulting images were processed in a Fujifilm BAS-5000 phosphor imager (Fujifilm, Tokyo, Japan). Analysis was performed using Multi Gauge 3.2 phosphor imager software (Fujifilm,

Tokyo, Japan). Specific binding was calculated by subtracting the level of nonspecific binding from the total binding for each section only considering the grey matter as the region of interest (ROI) for the quantification. ROIs were drawn manually on the autoradiogram using multigauge software and were used for the semiquantitative analyses. Graphs were created with GraphPad Prism 5.0 (GraphPad Software, Inc, San Diego, CA).

ACKNOWLEDGEMENTS

We would like to thank Dr Richard Lewis and Dr Gunnar Grönberg for the help with the NMR analysis and Dr Ryan Bragg for helpful discussions. This work was partially funded by the European Union's Horizon 2020 research and innovation programme under the Marie Sklodowska-Curie (H2020 Marie Sklodowska-Curie Actions) grant agreement 675417.

CONFLICT OF INTEREST

None declared.

FUNDING INFORMATION

H2020 Marie Sklodowska-Curie Actions, Grant/Award Number: 675417

ORCID

Markus Artelsmair https://orcid.org/0000-0002-2516-2925
Lee Kingston https://orcid.org/0000-0002-6845-6894
Charles S. Elmore https://orcid.org/0000-0001-7434-8307

REFERENCES

1. Lindley I, Westwick J, Kunkel S. Nomenclature announcement ± the chemokines. *Immunol Today*. 1993;14:24.
2. Baggiolini M. Chemokines in pathology and medicine. *J Intern Med*. 2001;250(2):91-104.
3. Murphy PM, Baggiolini M, Charo IF, et al. International union of pharmacology. XXII. Nomenclature for chemokine receptors. *Pharmacol Rev*. 2000;52(1):145-176.
4. Kunkel E, Butcher E. Homeostatic chemokines and the targeting of regional immunity. *Adv Exp Med Biol*. 2002;512:65-72.
5. Butcher EC, Picker LJ. Lymphocyte homing and homeostasis. *Science*. 1996;272(5258):60-67.
6. Bajetto A, Bonavia R, Barbero S, Florio T, Schettini G. Chemokines and their receptors in the central nervous system. *Front Neuroendocrinol*. 2001;22(3):147-184.
7. Lau BEK, Allen S, Hsu AR, Handel TM. Chemokine-receptor interactions: GPCRs, glycosaminoglycans and viral chemokine binding proteins. *Adv Protein Chem*. 2004;68:351-391.
8. Allen SJ, Crown SE, Handel TM. Chemokine:receptor structure, interactions, and antagonism. *Annu Rev Immunol*. 2007;25(1):787-820.
9. Boring L, Gosling J, Cleary M, Charo IF. Decreased lesion formation in CCR2(−/−) mice reveals a role for chemokines in the initiation of atherosclerosis. *Nature*. 1998;394(6696):894-897.
10. Dawson TC, Kuziel WA, Osahar TA, Maeda N. Absence of CC chemokine receptor-2 reduces atherosclerosis in apolipoprotein E-deficient mice. *Atherosclerosis*. 1999;143(1):205-211.
11. Tacke F, Alvarez D, Kaplan TJ, et al. Monocyte subsets differentially employ CCR2, CCR5, and CX3CR1 to accumulate within atherosclerotic plaques. *J Clin Investig*. 2007;117(1):185-194.
12. Mellado M, Martín de Ana A, Gómez L, Martínez C, Rodríguez-Frade JM. Chemokine receptor 2 blockade prevents asthma in a cynomolgus monkey model. *J Pharmacol Exp Ther*. 2008;324(2):769-775.
13. Lagu B, Gerchak C, Pan M, et al. Potent and selective CC-chemokine receptor-2 (CCR2) antagonists as a potential treatment for asthma. *Bioorg Med Chem Lett*. 2007;17(15):4382-4386.
14. Izikson BL, Klein RS, Charo IF, Weiner HL, Luster AD. Resistance to experimental autoimmune encephalomyelitis in mice lacking the CC chemokine receptor (CCR) 2. *J Exp Med*. 2000;192(7):1075-1080.
15. de Lema GP. Chemokine receptor CCR2 deficiency reduces renal disease and prolongs survival in MRL/lpr Lupus-prone mice. *J Am Soc Nephrol*. 2005;16(12):3592-3601.
16. Mahad DJ, Ransohoff RM. The role of MCP-1 (CCL2) and CCR2 in multiple sclerosis and experimental autoimmune encephalomyelitis (EAE). *Semin Immunol*. 2003;15(1):23-32.
17. Weisberg SP, Hunter D, Huber R, et al. CCR2 modulates inflammatory and metabolic effects of high-fat feeding. *J Clin Invest*. 2006;116(1):115-124.
18. Abbadie C, Lindia JA, Cumiskey AM, et al. Impaired neuropathic pain responses in mice lacking the chemokine receptor CCR2. *Proc Natl Acad Sci U S A*. 2003;100(13):7947-7952.
19. El Khoury J, Toft M, Hickman SE, et al. Ccr2 deficiency impairs microglial accumulation and accelerates progression of Alzheimer-like disease. *Nat Med*. 2007;13(4):432-438.
20. Carter PH, Cherney RJ, Mangion IK. Chapter 14 Advances in the discovery of CC chemokine receptor 2 antagonists. *Annu Rep Med Chem*. 2007;42:211-227.
21. Xia M, Sui Z. Recent developments in CCR2 antagonists. *Expert Opin Ther Pat*. 2009;19(3):295-303.
22. Struthers M, Pasternak A. CCR2 Antagonists. *Curr Top Med Chem*. 2010;10(13):1278-1298.
23. Schall TJ, Proudfoot AEI. Overcoming hurdles in developing successful drugs targeting chemokine receptors. *Nat Rev Immunol*. 2011;11(5):355-363.
24. Horuk R. Chemokine receptor antagonists: overcoming developmental hurdles. *Nat Rev Drug Discov*. 2009;8(1):23-33.

25. Hirsch L, Jette N, Frolkis A, Steeves T, Pringsheim T. The incidence of Parkinson's disease: a systematic review and meta-analysis. *Neuroepidemiology*. 2016;46(4):292-300.
26. Pringsheim T, Jette N, Frolkis A, Steeves TDL. The prevalence of Parkinson's disease: a systematic review and meta-analysis. *Mov Disord*. 2014;29(13):1583-1590.
27. Harms AS, Thome AD, Yan Z, et al. Peripheral monocyte entry is required for alpha-synuclein induced inflammation and neurodegeneration in a model of Parkinson disease. *Exp Neurol*. 2018;300:179-187.
28. Yao N, Wu Y, Zhou Y, et al. Lesion of the locus coeruleus aggravates dopaminergic neuron degeneration by modulating microglial function in mouse models of Parkinson's disease. *Brain Res*. 2015;1625:255-274.
29. Funk N, Wieghofer P, Grimm S, et al. Characterization of peripheral hematopoietic stem cells and monocytes in Parkinson's disease. *Mov Disord*. 2013;28(3):392-395.
30. Grozdanov V, Bliederhaeuser C, Ruf WP, et al. Inflammatory dysregulation of blood monocytes in Parkinson's disease patients. *Acta Neuropathol*. 2014;128(5):651-663.
31. Huerta C, Álvarez V, Mata IF, et al. Chemokines (RANTES and MCP-1) and chemokine-receptors (CCR2 and CCR5) gene polymorphisms in Alzheimer's and Parkinson's disease. *Neurosci Lett*. 2004;370(2-3):151-154.
32. Kalkonde YV, Morgan WW, Sigala J, et al. Chemokines in the MPTP model of Parkinson's disease: absence of CCL2 and its receptor CCR2 does not protect against striatal neurodegeneration. *Brain Res*. 2007;1128(1):1-11.
33. Yamasaki R, Yamaguchi H, Matsushita T, Fujii T, Hiwatashi A, Kira J. Early strong intrathecal inflammation in cerebellar type multiple system atrophy by cerebrospinal fluid cytokine/chemokine profiles: a case control study. *J Neuroinflammation*. 2017;14:1-10.
34. Lee W, Liao Y, Wang Y, Lin I, Wang S. Plasma MCP-1 and cognitive decline in patients with Alzheimer's disease and mild cognitive impairment: a two-year follow-up study. *Sci Rep*. 2018;8(1):1280.
35. Martin E, Delarasse C. Complex role of chemokine mediators in animal models of Alzheimer's disease. *Biomed J*. 2018;41(1):34-40.
36. Dimasi JA, Hansen RW, Grabowski HG. The price of innovation: new estimates of drug development costs. *J Health Economics*. 2003;22:151-185.
37. Adams CP, Brantner VV. Estimating the cost of new drug development: is it really $802 million? *Health Aff*. 2006;25(2):420-428.
38. Adams CP, Brantner VV. Spending on new drug development. *Health Econ*. 2010;19(2):130-141.
39. Kaitin KI, Dimasi JA. Pharmaceutical Innovation in the 21st Century: new drug approvals in the first decade, 2000-2009. *Clin Pharmacol Ther*. 2009;89:183-188.
40. Cumming JG, MacFaul PA, Leach AG. Novel N-thiazolyl piperazine-1-carboxamide CCR2 antagonists – investigation of an unexpected reaction with glutathione. *Med Chem Commun*. 2015;6(12):2140-2145.
41. Serrano A, Paré M, McIntosh F, et al. Blocking spinal CCR2 with AZ889 reversed hyperalgesia in a model of neuropathic pain. *Mol Pain*. 2010;6: 90:1744-8069.
42. Xue CB, Wang A, Han Q, et al. Discovery of INCB8761/PF-4136309, a potent, selective, and orally bioavailable CCR2 antagonist. *ACS Med Chem Lett*. 2011;2(12):913-918.
43. Xue CB, Feng H, Cao G, et al. Discovery of INCB3284, a potent, selective, and orally bioavailable hCCR2 antagonist. *ACS Med Chem Lett*. 2011;2(6):450-454.
44. Xia M, Hou C, DeMong D, et al. Substituted dipiperidine alcohols as potent CCR2 antagonists. *Bioorg Med Chem Lett*. 2008;18(12):3562-3564.
45. Xia M, Hou C, DeMong DE, et al. Synthesis, structure-activity relationship and in vivo antiinflammatory efficacy of substituted dipiperidines as CCR2 antagonists. *J Med Chem*. 2007;50(23):5561-5563.
46. Lipinski CA, Lombardo F, Dominy BW, Feeney PJ. Experimental and computational approaches to estimate solubility and permeability in drug discovery and development settings. *Adv Drug Deliv Rev*. 1997;23(1-3):3-25.
47. van der Born D, Sewing C, Herscheid J, et al. A Universal procedure for the [^{18}F]trifluoromethylation of aryl iodides and aryl boronic acids with highly improved specific activity. *Angew Chem Int Ed*. 2014;53(41):11046-11050.
48. Combadiere C, Ahuja SK, Lee Tiffany H, Murphy PM. Cloning and functional expression of CC CKR5, a human monocyte CC chemokine receptor selective for MIP-1α, MIP-1β, and RANTES. *J Leukoc Biol*. 1996;60(1):147-152.
49. Saljoughian M. Synthetic tritium labeling: reagents and methodologies. *Synthesis*. 2002;2002:1781-1801.
50. Voges R, Heys JR, Moenius T. *Preparation of Compounds Labeled with Tritium and Carbon-14*. Chicester: John Wiley & Sons Ltd; 2009.
51. O'Neil JP, VanBrocklin HF, Morimoto H, Williams PG. Synthesis of ^{3}H labeled dihydrorotenone. *J Label Compd Radiopharm*. 1997;39(3):215-221.
52. Berzelius JJ. Versuche, über die mit dem Platin vorkommenden Metalle, und über das Verfahren zur Zerlegung der natürlichen Platinlegirungen oder Platinerze. *Ann Phys*. 1828;89(7):435-488.
53. Felpin FX, Ayad T, Mitra S. Pd/C: An old catalyst for new applications—its use for the Suzuki-Miyaura reaction. *Eur J Org Chem*. 2006;2006(12):2679-2690.
54. Muzart J. Palladium-catalysed oxidation of primary and secondary alcohols. *Tetrahedron*. 2003;59(31):5789-5816.
55. Lamb GW, Watson AJA, Jolley KE, Maxwell AC, Williams JMJ. Borrowing hydrogen methodology for the conversion of alcohols into N-protected primary amines and in situ deprotection. *Tetrahedron Lett*. 2009;50(26):3374-3377.
56. Zhang Y, Qi X, Cui X, Shi F, Deng Y. Palladium catalyzed *N*-alkylation of amines with alcohols. *Tetrahedron Lett*. 2011;52(12):1334-1338.
57. Corma A, Ródenas T, Sabater MJ. A bifunctional PdVMgO solid catalyst for the one-pot selective *N*-monoalkylation of amines with alcohols. *Chem Eur J*. 2010;16(1):254-260.

58. Möhring VM, Fink G. Novel polymerization of α-olefins with the catalyst system nickel/aminobis (imino)phosphorane. *Angew Chem Int Ed Engl*. 1985;24(11):1001-1003.
59. Guo L, Dai S, Sui X, Chen C. Palladium and nickel catalyzed chain walking olefin polymerization and copolymerization. *ACS Catal*. 2016;6(1):428-441.
60. Culf AS, Morimoto H, Williams PG, Lockley WJS, Primrose WU, Jones JR. Synthesis of a tritium labelled phospholipase A2 inhibitor: a ligand for macromolecular ^{3}H NMR spectroscopy. *J Label Compd Radiopharm*. 1996;38(4):373-384.
61. Bähn S, Imm S, Neubert L, Zhang M, Neumann H, Beller M. The catalytic amination of alcohols. *Chem Cat Chem*. 2011;3(12):1853-1864.
62. Fulmer GR, Miller AJM, Sherden NH, et al. NMR chemical shifts of trace impurities: common laboratory solvents, organics, and gases in deuterated solvents relevant to the organometallic chemist. *Organometallics*. 2010;29(9):2176-2179.

How to cite this article: Artelsmair M, Miranda-Azpiazu P, Kingston L, et al. Synthesis, ^{3}H-labelling and in vitro evaluation of a substituted dipiperidine alcohol as a potential ligand for chemokine receptor 2. *J Label Compd Radiopharm*. 2019;62:265–279. https://doi.org/10.1002/jlcr.3731